Nano Research

Open Access

Research Article

Synergistic modulation of oxygen vacancies and confinement effects in CeO_2 for high-selectivity synthesis of azoxyarenes

Wenwen Chen[1] ✉, Chenyang Gao[1], Jingyu Li[1], Xiaomei Liu[1], Xiao Liang[2] ✉, and Jianfeng Jia[1] ✉

[1] *Shanxi Center of Technology Innovation for Advanced Power Battery Material, School of Chemistry and Chemical Engineering, Shanxi Normal University, Taiyuan 030031, China*
[2] *Department of Chemistry, Tsinghua University, Beijing 100084, China*

Cite this article: *Nano Research*, **2026**, *19*, 94908483. https://doi.org/10.26599/NR.2026.94908483

ABSTRACT: The selective reduction of nitrobenzene is considered the primary route for synthesizing azoxybenzene, yet this process often suffers from over-reduction, resulting in low selectivity toward the target product. Achieving efficient N–N coupling of key intermediates thus remains a central challenge for improving selectivity. To address this, we prepared a series of oxygen-vacancy-rich CeO_2 nanosphere catalysts by modulating acetic acid concentration and temperature during hydrothermal synthesis. These catalysts exhibit high specific surface areas (up to 184.1 $m^2 \cdot g^{-1}$) and demonstrate excellent performance in the highly selective reduction of nitrobenzene to azoxybenzene. Mechanistic studies reveal that oxygen vacancies on the CeO_2 surface promote the condensation of nitrosobenzene and phenylhydroxylamine into azoxybenzene via a confinement effect. Moreover, X-ray photoelectron spectroscopy (XPS) analysis shows that azoxybenzene adsorbs much more weakly on the catalyst surface than nitrobenzene or aniline, favoring its rapid desorption and thereby suppressing further reduction. This work clarifies how oxygen vacancies in confined microenvironments on CeO_2 enhance the N–N coupling pathway, providing important theoretical and experimental guidance for designing highly selective catalytic systems for nitroarene reduction.

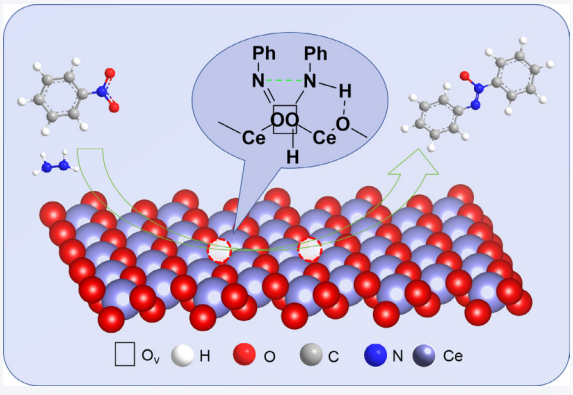

KEYWORDS: oxygen vacancies, confinement effect, ceria dioxide, nitroarene reduction

1 Introduction

Azoxybenzene, distinguished by its characteristic –N=N(O)– functional group, serves as a central building block in both naturally occurring compounds [1] and synthetic functional materials [2, 3]. It is extensively utilized in the synthesis of pharmaceuticals [4–6], agrochemicals [7], and liquid crystal materials [8, 9]. Currently, the primary synthetic methods for azoxybenzene include the reduction of nitrobenzene [10–14] and the oxidation of aniline [15–19]. These approaches often involve harsh conditions, rely on noble metal catalysts, or generate substantial waste. Therefore, developing green, efficient, and highly selective catalytic synthetic routes is not only an inherent need for upgrading the fine chemical industry but also holds significant strategic importance in achieving the carbon neutrality goals.

Azoxybenzene is most commonly produced industrially via the selective reduction of nitrobenzene. This multi-step reduction proceeds through intermediates such as nitrosobenzene, phenylhydroxylamine, and azobenzene, ultimately yielding aniline. However, in most conventional catalytic systems, the reaction readily proceeds beyond the azoxybenzene stage toward deeper hydrogenation, resulting in low selectivity for the target product [20–22]. Therefore, how to precisely control the reaction progress, suppress over-reduction, and effectively promote N–N coupling between key intermediates such as nitrosobenzene or phenylhydroxylamine to achieve high-selectivity synthesis of azoxybenzene remains a long-standing core challenge and a key scientific issue in this field.

In recent years, cerium dioxide (CeO_2), as a common metal oxide, has attracted widespread attention due to its excellent redox properties [23, 24]. The fluorite structure and abundant surface defects of CeO_2 collectively facilitate the efficient and reversible

Received: December 30, 2025; **Revised:** January 16, 2026
Accepted: January 21, 2026

✉Address correspondence to Wenwen Chen, chenww@sxnu.edu.cn; Xiao Liang, liangx1996@outlook.com; Jianfeng Jia, jiajf@dns.sxnu.edu.cn

conversion between Ce^{4+} and Ce^{3+}, thereby endowing it with tunable redox characteristics. In this process, oxygen vacancies (O_v) serve as key active sites, directly participating in and driving the adsorption and activation of reactants, demonstrating unique advantages in the selective transformation of nitroarenes. For instance, Ren et al. [25] developed the dual-site Pt/CeO_2 catalyst to convert sulfur-containing nitroarenes. In this system, the O_v on the CeO_2 support are designed to directly activate nitro groups, whereas the Pt metal sites are dedicated solely to activating hydrogen via the hydrogen spillover effect. This strategy successfully achieves efficient conversion of sulfur-containing nitroarenes while effectively avoiding sulfur poisoning issues. Similarly, Zhang et al. [26] reported the Ag_1-Pd_1/CeO_2 dual-atom catalyst, where O_v on the CeO_2 surface synergize with the dual-atom sites to promote the coupling condensation of nitroarenes and further guide the efficient conversion of condensation intermediates into aromatic amines.

Although O_v serve as crucial active sites capable of efficiently activating nitro-substrates, relying solely on their electronic effects is often insufficient for precisely controlling the regioselectivity and chemoselectivity of coupling steps. By constructing atomically dispersed dual sites, the confinement effect can impose both spatial and electronic constraints, enabling nitro-derived intermediates to align directionally in close proximity [27, 28]. This significantly enhances the probability of N–N coupling while suppressing side reactions. Integrating confinement structures with the activation function of O_v holds promise for multidimensional modulation of reaction pathways, offering a new catalytic platform for the highly selective synthesis of compounds containing N–N bonds.

Based on this, the present study prepared a series of oxygen vacancy-rich CeO_2 nanosphere catalysts by modulating the acetic acid addition and reaction temperature in hydrothermal synthesis. This series of catalysts possesses a high specific surface area (up to 184.1 m^2/g), exhibits excellent catalytic performance in the catalytic reduction of nitrobenzene, and demonstrates good tolerance toward substrates with various substituted functional groups. Mechanistic studies indicate that O_v on the CeO_2 surface promote the condensation of nitrosobenzene and phenylhydroxylamine to efficiently form azoxybenzene through a confinement effect. X-ray photoelectron spectroscopy (XPS) analysis further reveals that the adsorption strength of azoxybenzene on the catalyst surface is significantly lower than that of nitrobenzene and aniline. This weaker adsorption favors rapid product desorption, thereby effectively inhibiting its further reduction. This work elucidates the promotion mechanism of CeO_2 surface O_v on the N–N coupling pathway under a confined microenvironment, providing important theoretical and experimental foundations for the design of selective reduction catalytic systems for nitroarenes.

2 Experimental

2.1 Preparation of catalysts

In a typical synthesis, 3 g of $Ce(NO_3)_3{\cdot}6H_2O$ was dissolved in 2 mL of deionized water under ultrasonic dispersion. Then, 4 mL of glacial acetic acid and 40 mL of ethylene glycol were added to the mixture, which was stirred continuously for 30 min. The resulting solution was transferred into a Teflon-lined autoclave and subjected to hydrothermal treatment at 160 °C for 220 min. After the reaction, the product was collected and washed repeatedly with deionized water and ethanol, followed by drying at 60 °C for 8 h in a vacuum oven. Finally, CeO_2 nanospheres were obtained after calcination at 500 °C for 1 h. The specific surface area of the CeO_2 nanospheres was modulated by varying the amount of glacial acetic acid and the hydrothermal temperature. The catalysts prepared with different volumes of acetic acid (2, 3, 4, and 5 mL) were denoted as CeO_2-2mL, CeO_2-3mL, CeO_2-4mL, and CeO_2-5mL, respectively. Similarly, samples synthesized at different hydrothermal temperatures (140, 160, and 180 °C) were labeled as CeO_2-140°C, CeO_2-160°C, and CeO_2-180°C.

2.2 Characterization

The microstructure and crystal structure of the catalyst were analyzed by scanning electron microscopy (SEM), transmission electron microscopy (TEM), and X-ray diffraction (XRD). The surface elements of the catalysts were analyzed by XPS. The O_v of the catalyst were analyzed by electron spin paramagnetic resonance (EPR) spectroscopy. The reaction pathway was explored by *in situ* infrared spectroscopy.

2.3 Catalytic performance test

A typical catalytic test was conducted in a 10 mL Schlenk tube. The reaction mixture containing 25 mg of catalyst, 0.3 mmol of nitrobenzene, 0.75 mmol of hydrazine hydrate ($N_2H_4{\cdot}H_2O$), and 4 mL of acetonitrile was first stirred in the dark for 15 min to achieve adsorption–desorption equilibrium. The reaction was then performed at 60 °C for 2 h under a N_2 atmosphere. After completion, the reaction was quenched with deionized water and extracted with dichloromethane. The organic phase was collected and analyzed by gas chromatography to determine substrate conversion and product selectivity.

3 Results and discussion

3.1 Catalyst characterization

CeO_2 with high specific surface area was prepared by a simple solvothermal method, and the microstructure and crystal structure of the catalyst were characterized by SEM, TEM, and high-resolution TEM (HRTEM). From the characterization results (Figs. 1(a)–1(c)), CeO_2 exhibits a uniform nanosphere morphology with a size of about 180 nm. In the TEM images, the 0.32 nm lattice spacing belongs to the (111) facet of CeO_2 (Fig. 1(c)) [29]. The above characterization proves the successful preparation of CeO_2 catalyst.

The crystal structure and surface defects of the CeO_2 catalysts were further characterized by XRD and EPR. As shown in Figs. 1(d) and 1(e), all the synthesized CeO_2 samples exhibit characteristic diffraction peaks consistent with the fluorite structure of CeO_2 (JCPDS No. 34-0394) [30], confirming the successful formation of the target phase. Notably, the sample prepared with 4 mL of acetic acid at a hydrothermal temperature of 160 °C showed sharper and more intense diffraction peaks, suggesting improved crystallinity under these conditions. Furthermore, the EPR spectrum (Fig. 1(f)) displays a distinct signal at 2.03, which is characteristic of O_v, confirming their presence in the CeO_2 catalysts [31].

The surface chemical composition and oxidation states of the CeO_2 catalysts were further examined by XPS (Fig. 1(g)). As shown in Fig. 1(h), the high-resolution Ce 3d spectrum can be deconvoluted into multiple characteristic peaks. Specifically, the

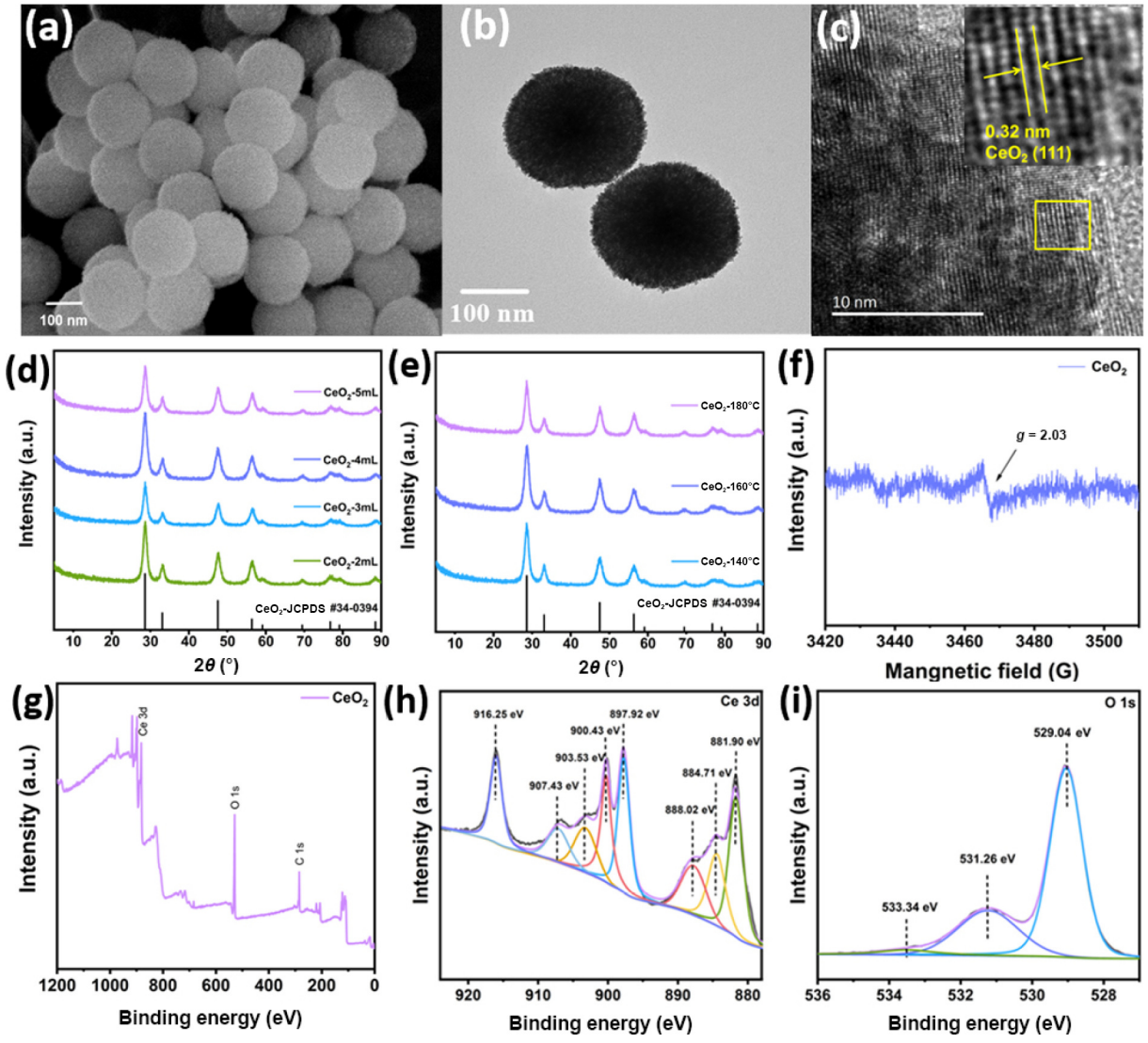

Figure 1 (a) SEM image, (b) TEM image, and (c) HRTEM image of CeO_2. (d) XRD patterns of CeO_2 prepared with different amounts of glacial acetic acid. (e) XRD spectra of CeO_2 prepared at different hydrothermal temperatures. (f) EPR spectrum of CeO_2. (g) XPS survey spectrum of CeO_2. (h) Ce 3d XPS spectrum of CeO_2. (i) O 1s XPS spectrum of CeO_2.

peaks located at 900.43, 903.53, 907.43, and 916.25 eV are assigned to the Ce $3d_{3/2}$ level, while those at 881.90, 884.71, 888.02, and 897.92 eV correspond to the Ce $3d_{5/2}$ level. This spectral profile confirms the coexistence of both Ce^{3+} and Ce^{4+} oxidation states in the CeO_2 sample. Furthermore, the O 1s spectrum (Fig. 1(i)) was fitted into three components centered at binding energies of 529.04, 531.26, and 533.34 eV, which are attributed to lattice oxygen, oxygen species associated with O_v, and surface-adsorbed hydroxyl groups, respectively [32, 33].

It is well established that the specific surface area significantly influences the catalytic activity. Generally, a larger specific surface area provides more adsorption and active sites, which is conducive to enhancing catalyst performance [34]. In this study, we modulated the specific surface area of CeO_2 catalysts by varying the amount of acetic acid and the hydrothermal temperature. The textural properties of the synthesized CeO_2 series were characterized by N_2 adsorption–desorption measurements. As illustrated in Figs. S1(a) and S1(b) in the Electronic Supplementary Material (ESM), the N_2 adsorption–desorption isotherms of the modified catalysts exhibit a typical Type IV characteristic [35], indicative of mesoporous materials. This is further corroborated by the pore size distribution profiles (Figs. S1(c) and S1(d) in the ESM), which reveal that the pore structure of CeO_2 was effectively modulated, showing a well-defined mesoporous architecture. As summarized in Table S1 in the ESM, the specific surface area of the CeO_2 catalyst could be significantly enhanced through the optimization of acetic acid content and hydrothermal temperature, achieving a maximum value of 184.1 m^2/g.

3.2 Study on catalytic performance

The catalytic performance of the synthesized CeO_2 materials was initially evaluated in the reduction of nitrobenzene to azoxybenzene at 60 °C under a N_2 atmosphere for 4 h. As shown in Figs. 2(a) and 2(b), the CeO_2-4mL, CeO_2-160°C, and CeO_2-180°C catalysts demonstrated optimal performance under these conditions, achieving a nitrobenzene conversion of 99% with an azoxybenzene selectivity of 90%. To further investigate the performance differences between the two catalysts, the reaction time was

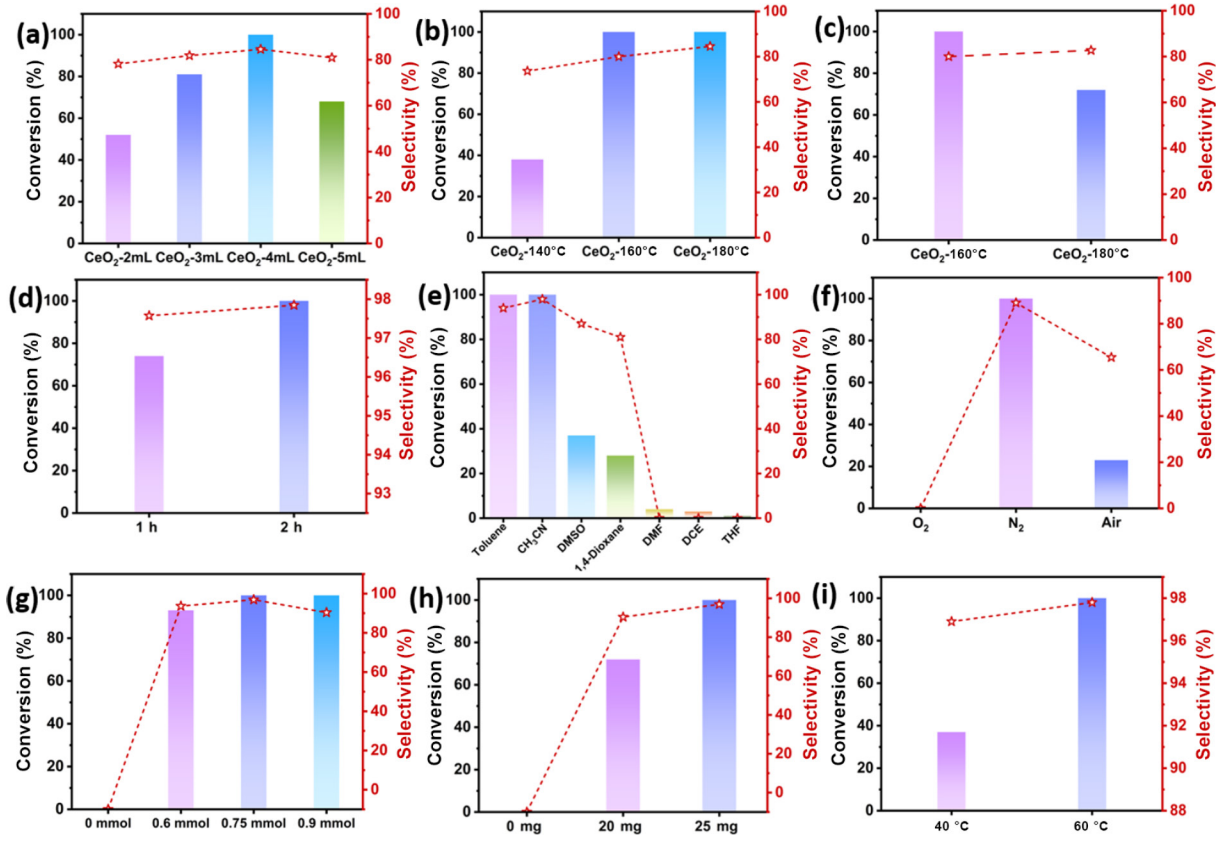

Figure 2 Screening (a) the amount of acid and ((b) and (c)) hydrothermal temperature of CeO_2 catalyst. The effects of (d) reaction time, (e) solvent, (f) atmosphere, (g) $N_2H_4{\cdot}H_2O$ amount, (h) catalyst loading on the reduction of nitrobenzene, and (i) reaction temperature.

shortened to 3 h for comparison between CeO_2-160°C and CeO_2-180°C. The results revealed that CeO_2-160°C maintained superior activity, with 99% conversion and 89% selectivity (Fig. 2(c)). This performance trend is consistent with the Brunauer–Emmett–Teller (BET) surface area measurements, indicating that a larger surface area facilitates the nitrobenzene reduction reaction. Consequently, the catalyst synthesized with 4 mL of acetic acid at 160 °C (denoted as CeO_2 hereafter) was selected for all subsequent tests.

Subsequently, a detailed investigation was conducted to evaluate the effects of reaction time, solvent, equivalent ratio, catalyst loading, atmosphere, and temperature on the nitrobenzene reduction. The reaction time was first optimized. When the time was shortened to 2 h, nitrobenzene conversion (> 99%) and azoxybenzene selectivity (98%) reached their optimum values. A further reduction to 1 h led to a significant decrease in conversion (74%). Therefore, 2 h was selected as the standard reaction time (Fig. 2(d)). The solvent was found to have a profound impact on the reaction efficacy. The use of tetrahydrofuran (THF), N,N-dimethylformamide (DMF), or 1,2-dichloroethane (DCE) markedly impeded the reaction, yielding minimal nitrobenzene conversion, which can be ascribed to insufficient catalyst dispersion. Although toluene enabled a high conversion (> 99%) and a selectivity of 94% to azoxybenzene, acetonitrile proved superior with a selectivity of 98%. Consequently, acetonitrile was chosen for all follow-on investigations (Fig. 2(e)). Replacing N_2 with air resulted in a significant drop in conversion (23%), and under an O_2 atmosphere, the reaction was completely suppressed, indicating the inhibitory effect of oxygen (Fig. 2(f)). Control experiments confirmed that both the catalyst and hydrazine hydrate are essential for the reaction to proceed (Figs. 2(g) and 2(h)). Varying the amount of $N_2H_4{\cdot}H_2O$ to 0.6 or 0.9 mmol led to decreased selectivity toward azoxybenzene. Increasing the hydrazine equivalent promoted over-reduction to azobenzene or aniline, thereby reducing the selectivity for azoxybenzene (92%). Finally, lowering the reaction temperature to 40 °C resulted in a conversion of only 37% (Fig. 2(i)), confirming that 60 °C is more suitable for this transformation. The optimal reaction conditions were established as follows: Nitrobenzene (0.3 mmol), hydrazine hydrate (0.75 mmol), CeO_2 (25 mg), and acetonitrile (4 mL) were reacted under N_2 at 60 °C for 2 h. Under these optimized conditions, the CeO_2-catalyzed reduction of nitrobenzene achieved a conversion of 99% with a selectivity of 98% for azoxybenzene. This performance compares favorably with previously reported systems, highlighting the superior efficiency of the present CeO_2 catalyst (Table S2 in the ESM).

Under the optimal conditions, the functional group tolerance of the CeO_2-catalyzed nitrobenzene reduction was investigated. As summarized in Table 1, excellent conversion and selectivity were achieved for substrates bearing either electron-withdrawing or electron-donating groups, demonstrating the remarkable substrate generality of the CeO_2 catalyst for the reduction of nitrobenzene to azoxybenzene. However, a significant yield reduction (21%–71%) was observed for ortho-substituted substrates, indicating that steric hindrance is a decisive factor influencing the reaction.

3.3 Stability test and analysis of catalyst

Stability is a critical performance metric for catalysts and holds paramount importance in guiding their design. To this end, we

Table 1 Nitrobenzene reduction substrate expansion[a]

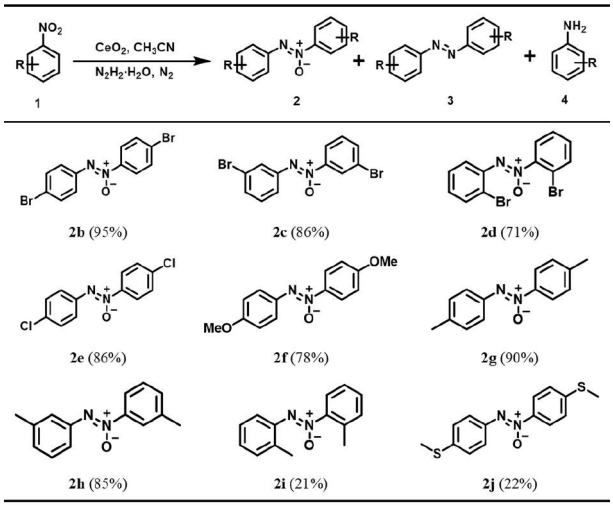

[a]Reaction conditions: nitrobenzene (0.3 mmol), $N_2H_4{\cdot}H_2O$ (0.75 mmol), catalyst (25 mg), solvent (4 mL), and reaction for 2 h.

evaluated the CeO_2 catalyst for its cycling stability. As shown in Fig. 3(a), after three consecutive reaction cycles, the selectivity for the reduction of nitrobenzene to azoxybenzene remained largely unchanged, while the conversion rate exhibited a marginal drop. To investigate the cause of this performance decay, cycled catalyst was characterized by XRD (Fig. 3(b)), XPS (Figs. 3(c)–3(e)), SEM (Fig. S2 in the ESM), and Fourier transform infrared (FTIR) (Fig. 3(f)). The SEM, XRD, and FTIR results indicated no significant changes in the morphology or crystal structure of CeO_2 after cycling, demonstrating its robust structural stability under reaction conditions. Further XPS analysis revealed that the chemical states of Ce and O elements remained essentially consistent before and after the reaction. However, N 1s peaks were detected in the spent catalyst, with binding energies at 404.48 and 399.33 eV, attributable to the nitro nitrogen from nitrobenzene and the amino nitrogen from aniline, respectively [36]. These observations suggest that incompletely converted nitrobenzene and a small amount of the by-product aniline may adsorb and remain on the CeO_2 surface, thereby covering some active sites and leading to the gradual decline in catalytic performance. Furthermore, only adsorbed species of nitrobenzene and aniline were detected on the CeO_2 surface, while no other intermediates or azoxybenzene were captured. This indicates that the adsorption energy of the latter on CeO_2 is significantly lower than that of nitrobenzene and aniline, allowing azoxybenzene to desorb more readily from the catalyst surface once formed, thereby avoiding its excessive adsorption and further conversion.

3.4 Reduction mechanism of nitrobenzene

At present, there are two reduction pathways of nitrobenzene proposed in the literature (Fig. S3 in the ESM). First, nitrobenzene is reduced to nitrosobenzene and phenyl hydroxylamine, and then different reaction pathways occur (Fig. S3 in the ESM). In the first pathway, nitrosobenzene and phenyl hydroxylamine are coupled to form azobenzene oxide, which then further reacts to form azobenzene, and the second route is the direct formation of aniline from nitrobenzene and phenylhydroxylamine without coupling [37].

To elucidate the reaction pathway and the origin of selectivity in the CeO_2-catalyzed reduction of nitrobenzene, a series of mechanistic experiments were conducted. First, to examine whether azoxybenzene could be formed via the oxidation of aniline, a control experiment was performed using aniline as the substrate under standard conditions (Fig. S4 in the ESM). The results showed no formation of azoxybenzene, thus ruling out the pathway involving aniline oxidation. To further confirm the reaction route,

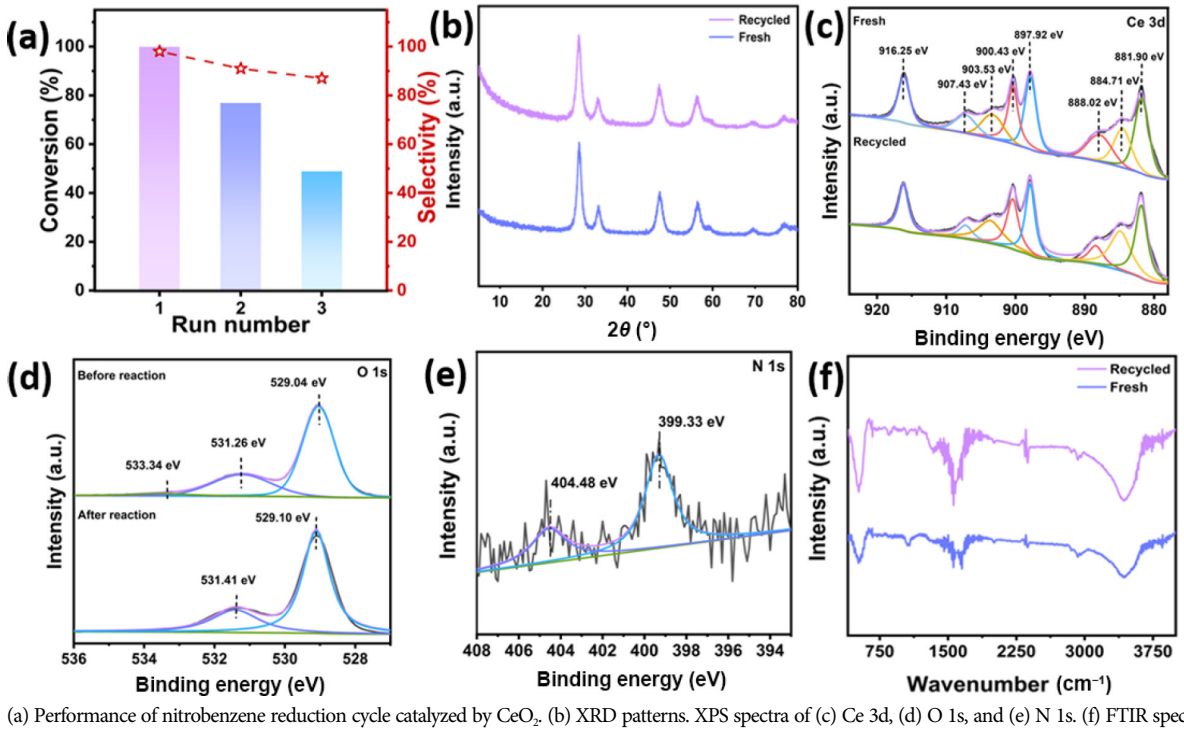

Figure 3 (a) Performance of nitrobenzene reduction cycle catalyzed by CeO_2. (b) XRD patterns. XPS spectra of (c) Ce 3d, (d) O 1s, and (e) N 1s. (f) FTIR spectra before and after CeO_2 stability test.

in situ FTIR spectroscopy was employed to monitor the nitrobenzene reduction process. As shown in Fig. 4(a), the absorption peaks at 1380 and 1558 cm^{-1} are attributed to the asymmetric stretching vibrations of the $-NO_2$ group in nitrobenzene. The peak at 1184 cm^{-1} is assigned to the N–O stretching vibration of phenylhydroxylamine, while the signal at 1426 cm^{-1} corresponds to the N=O stretching vibration in nitrosobenzene or the –N=N–O stretching vibration in azoxybenzene [38, 39]. These results indicate the presence of nitrosobenzene and phenylhydroxylamine intermediates during the CeO_2-catalyzed reduction of nitrobenzene and confirm that azoxybenzene is formed via N–N coupling between these two intermediates. Notably, in many catalytic systems, the N–N coupling step is unfavorable, and the reduction of nitrobenzene often stops at the phenylhydroxylamine [39, 40] or proceeds further to aniline [20, 21]. We propose that the abundant O_v on the CeO_2 surface play a key role in directing the selective formation of azoxybenzene. The O_v can strongly adsorb the oxygen atoms of nitrosobenzene and phenylhydroxylamine in a vacancy-filling manner, thereby significantly increasing the proximity and interaction between the two intermediates and promoting their coupling reaction.

Subsequently, we further investigated the influence of reaction time on the product distribution to examine whether prolonged reaction time would lead to the over-reduction of azoxybenzene to azobenzene or aniline. As shown in Fig. 4(b), both the nitrobenzene conversion (> 99%) and the selectivity toward azoxybenzene (98%) reached their maximum values at a reaction time of 2 h. Even when the reaction was extended to 5 h, the selectivity to azoxybenzene remained at 84%, showing only a minor decrease. These results indicate that, within this catalytic system, azoxybenzene does not undergo significant side reactions to form azobenzene or aniline over extended time, confirming its good stability under the reaction conditions. Combined with the XPS results of CeO_2 after three cycles, we propose that the reaction stops at the azoxybenzene stage and does not proceed further to aniline likely because of the weak adsorption of azoxybenzene on CeO_2, which inhibits its subsequent reduction to azobenzene or aniline [41, 42].

Based on the experimental results above, we propose a reaction mechanism, as illustrated in Fig. 5. Under heating, the O_v on the CeO_2 surface preferentially adsorb and activate the nitrobenzene molecule [22]. Subsequently, the active hydrogen species released from hydrazine hydrate attack the activated nitrobenzene [43], reducing it to a nitrosobenzene intermediate. This intermediate is further hydrogenated on CeO_2 to form phenylhydroxylamine.

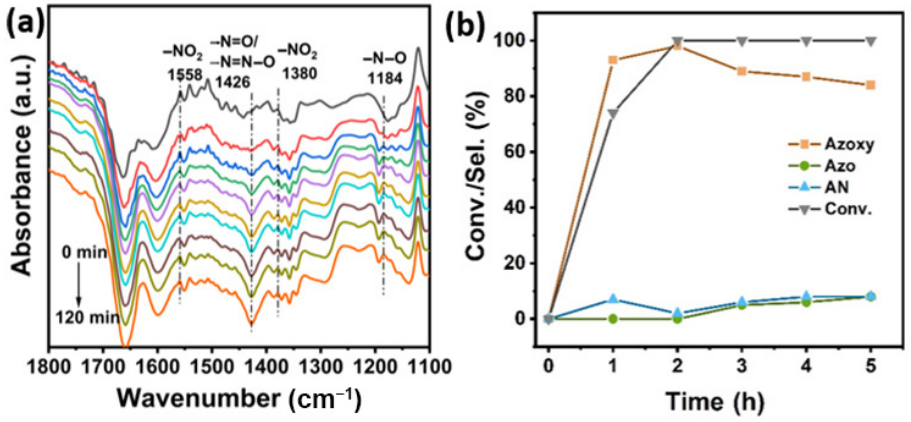

Figure 4 (a) *In situ* infrared spectra of nitrobenzene reduction catalyzed by CeO_2. (b) Distribution of nitrobenzene reduction products catalyzed by CeO_2 over time.

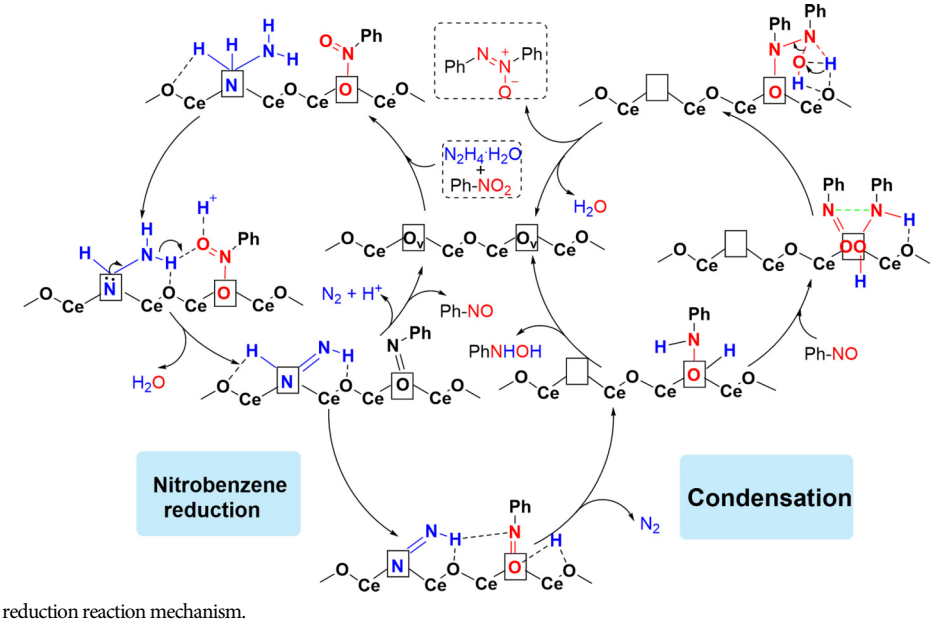

Figure 5 Nitrobenzene reduction reaction mechanism.

Through the spatial confinement effect of the O_v, nitrosobenzene and phenylhydroxylamine are confined to adjacent active sites, where they undergo dehydration coupling to generate the target product, azoxybenzene [44, 45].

Due to its relatively large steric hindrance, the interaction between azoxybenzene and O_v weakens significantly, allowing it to desorb rapidly from the catalyst surface and preventing further reduction to aniline. Moreover, the O_v sites are regenerated and enter the next catalytic cycle. The stable concentration of O_v before and after the reaction (Fig. S5 in the ESM) further confirms the effectiveness of this confinement–coupling–desorption dynamic mechanism.

4 Summary

In summary, this study successfully prepared high-specific-surface-area CeO_2 nanosphere catalysts rich in O_v by modulating hydrothermal conditions. These catalysts achieved a conversion of > 99% and an azoxybenzene selectivity of 98% in the nitrobenzene reduction reaction, while also demonstrating excellent substrate universality. Mechanistic studies indicate that the surface O_v promote the condensation of key intermediates to form N=N bonds through a confinement effect, while the weak adsorption characteristic of azoxybenzene effectively inhibits its deep reduction. This work not only reveals the dual role of O_v in regulating the reaction pathway and product selectivity but also provides a referable strategy and theoretical support for designing efficient and highly selective non-noble metal oxide catalysts.

Electronic Supplementary Material: Supplementary material (N_2 adsorption–desorption isotherms and pore size distributions of CeO_2 catalysts, SEM after CeO_2 stability test, nitrobenzene reduction mechanism diagram, EPR spectrum after CeO_2 stability test, and NMR characterization of the products and supplementary tables) is available in the online version of this article at https://doi.org/10.26599/NR.2026.94908483.

Data availability

All data needed to support the conclusions in the paper are presented in the manuscript and the Electronic Supplementary Material. Additional data related to this paper may be requested from the corresponding author upon request.

Acknowledgements

This work was supported by the Joint Funds Project of the National Natural Science Foundation of China (No. U24A2023), Fundamental Research Program of Shanxi Province (No. 202503021211188), and the China Postdoctoral Science Foundation (No. 2025M770993).

Declaration of competing interest

All the contributing authors report no conflict of interests in this work.

Author contribution statement

W. W. C.: Data curation, project administration, validation, writing manuscript, experimental design, funding acquisition. C. Y. G.: Data curation, validation, experimental design. J. Y. L.: Data curation, validation. X. M. L.: Data curation, validation. X. L.: Project administration, funding acquisition, writing manuscript. J. F. J.: Project administration, funding acquisition, writing manuscript. All the authors have approved the final manuscript.

Use of AI statement

None.

References

[1] Garg, R. P.; Alemany, L. B.; Moran, S.; Parry, R. J. Identification, characterization, and bioconversion of a new intermediate in valanimycin biosynthesis. *J. Am. Chem. Soc.* **2009**, *131*, 9608–9609.

[2] He, H. Y.; Niikura, H.; Du, Y. L.; Ryan, K. S. Synthetic and biosynthetic routes to nitrogen-nitrogen bonds. *Chem. Soc. Rev.* **2022**, *51*, 2991–3046.

[3] Folcia, C. L.; Alonso, I.; Ortega, J.; Etxebarria, J.; Pintre, I.; Ros, M. B. Achiral bent-core liquid crystals with Azo and azoxy linkages: Structural and nonlinear optical properties and photoisomerization. *Chem. Mater.* **2006**, *18*, 4617–4626.

[4] Cai, B. G.; Empel, C.; Yao, W. Z.; Koenigs, R. M.; Xuan, J. Azoxy compounds-from synthesis to reagents for azoxy group transfer reactions. *Angew. Chem., Int. Ed.* **2023**, *62*, e202312031.

[5] De Padua, J. C.; Tanaka, T.; Ueno, K.; Dela Cruz, T. E. E.; Ishihara, A. Isolation of 2,2′-azoxybisbenzyl alcohol from *Agaricus subrutilescens* and its inhibitory activity against bacterial biofilm formation. *Biosci. Biotechnol. Biochem.* **2024**, *88*, 983–991.

[6] Wibowo, M.; Ding, L. Chemistry and biology of natural azoxy compounds. *J. Nat. Prod.* **2020**, *83*, 3482–3491.

[7] Sugawara, A.; Kubo, M.; Hirose, T.; Yahagi, K.; Tsunoda, N.; Noguchi, Y.; Nakashima, T.; Takahashi, Y.; Welz, C.; Mueller, D. et al. Jietacins, azoxy antibiotics with potent nematocidal activity: Design, synthesis, and biological evaluation against parasitic nematodes. *Eur. J. Med. Chem.* **2018**, *145*, 524–538.

[8] Vix, A. B. E.; Müller-Buschbaum, P.; Stocker, W.; Stamm, M.; Rabe, J. P. Crossover between dewetting and stabilization of ultrathin liquid crystalline polymer films. *Langmuir* **2000**, *16*, 10456–10462.

[9] Scherschel, N. F.; Piercey, D. G. Nitrodiazene oxides: A unique nitrogen- and oxygen-containing functional group. *Roy. Soc. Open Sci.* **2024**, *11*, 231935.

[10] Dai, Y. T.; Li, C.; Shen, Y. B.; Lim, T.; Xu, J.; Li, Y. W.; Niemantsverdriet, H.; Besenbacher, F.; Lock, N.; Su, R. Light-tuned selective photosynthesis of azo- and azoxy-aromatics using graphitic C_3N_4. *Nat. Commun.* **2018**, *9*, 60.

[11] Doherty, S.; Knight, J. G.; Backhouse, T.; Summers, R. J.; Abood, E.; Simpson, W.; Paget, W.; Bourne, R. A.; Chamberlain, T. W.; Stones, R. et al. Highly selective and solvent-dependent reduction of nitrobenzene to *N*-phenylhydroxylamine, azoxybenzene, and aniline catalyzed by phosphino-modified polymer immobilized ionic liquid-stabilized AuNPs. *ACS Catal.* **2019**, *9*, 4777–4791.

[12] Gong, W. B.; Mao, X.; Zhang, J. F.; Lin, Y.; Zhang, H. M.; Du, A. J.; Xiong, Y. J.; Zhao, H. J. Ni-Co alloy nanoparticles catalyze selective electrochemical coupling of nitroarenes into azoxybenzene compounds in aqueous electrolyte. *ACS Nano* **2023**, *17*, 3984–3995.

[13] Li, Z. J.; Lu, X. W.; Guo, C.; Ji, S. Q.; Liu, H. X.; Guo, C. M.; Lu, X.; Wang, C.; Yan, W. S.; Liu, B. Y. et al. Solvent-free selective hydrogenation of nitroaromatics to azoxy compounds over Co single atoms decorated on Nb_2O_5 nanomeshes. *Nat. Commun.* **2024**, *15*, 3195.

[14] Zhang, J. Z.; Zhang, Y. B.; Chai, H. L.; Luo, H. L.; Du, C. X.; Huang, R. W.; Zang, S. Q. Selectivity modulation of multistep reduction reactions by gold nanoclusters. *Angew. Chem., Int. Ed.* **2025**, *64*, e202413418.

[15] Arango-Daza, J. C.; Onillon, M.; Nork, L.; Mopoung, K.; Puttisong,

Y.; Rivero-Crespo, M. A. Metal-organic framework/organocatalyst combinations as powerful multicatalytic systems for aerobic oxidations. *Angew. Chem., Int. Ed.* **2026**, *65*, e23426.
[16] Grirrane, A.; Corma, A.; García, H. Gold-catalyzed synthesis of aromatic Azo compounds from anilines and nitroaromatics. *Science* **2008**, *322*, 1661–1664.
[17] Han, S.; Cheng, Y.; Liu, S. S.; Tao, C. F.; Wang, A. P.; Wei, W. G.; Yu, H.; Wei, Y. G. Selective oxidation of anilines to azobenzenes and azoxybenzenes by a molecular Mo oxide catalyst. *Angew. Chem., Int. Ed.* **2021**, *60*, 6382–6385.
[18] Qin, J. H.; Long, Y.; Sun, F. K.; Zhou, P. P.; Wang, W. D.; Luo, N.; Ma, J. T. $Zr(OH)_4$-catalyzed controllable selective oxidation of anilines to azoxybenzenes, azobenzenes and nitrosobenzenes. *Angew. Chem., Int. Ed.* **2022**, *61*, e202112907.
[19] Tanini, D.; Dalia, C.; Capperucci, A. The polyhedral nature of selenium-catalysed reactions: Se(IV) species instead of Se(VI) species make the difference in the on water selenium-mediated oxidation of arylamines. *Green Chem.* **2021**, *23*, 5680–5686.
[20] Bal, M.; Van Hoey, W.; Cleirbaut, R.; Lemière, F.; Van Doorslaer, S.; Cool, P.; Maes, B. U. W. Visible light-photoinduced and Cu-catalyzed reduction of nitrobenzenes into anilines. *ACS Catal.* **2025**, *15*, 4726–4738.
[21] Ran, P.; Wei, F. F.; Xiang, B. Y.; Qiu, A. Q.; Tian, B. L.; Xu, X. R.; Dai, L. H.; Zhang, H. W.; Wang, F. Y.; Sun, Y. M. et al. Efficient, versatile, and durable electrocatalytic nitroaromatic-to-arylamine reduction via heteroatom-site hydrogen-atom transfer. *J. Am. Chem. Soc.* **2025**, *147*, 37414–37427.
[22] Zheng, X. H.; Li, B.; Huang, R.; Jiang, W. P.; Shen, L. J.; Lei, G. C.; Wang, S. P.; Zhan, Y. Y.; Jiang, L. L. Asymmetric oxygen vacancy-promoted synthesis of aminoarenes from nitroarenes using waste H_2S as a "hydrogen donor". *ACS Catal.* **2024**, *14*, 10245–10259.
[23] Khivantsev, K.; Pham, H.; Engelhard, M. H.; Aleksandrov, H. A.; Kovarik, L.; Bowden, M.; Li, X. S.; Tian, J. S.; Koleva, I. Z.; Song, I. et al. Transforming ceria into 2D clusters enhances catalytic activity. *Nature* **2025**, *640*, 947–953.
[24] Yang, J.; Falling, L. J.; Yan, S. Y.; Zhang, B. L.; Verma, P.; Daemen, L.; Cheng, Y. Q.; Zhao, X.; Zhang, S. C.; Chen, J. L. et al. Formation of hydrided Pt-Ce-H sites in efficient, selective oxidation catalysts. *Science* **2025**, *388*, 514–519.
[25] Ren, X. M.; Huang, J. Y.; Ma, J.; Zhang, Y. M.; Chu, W.; Perathoner, S.; Centi, G.; Liu, Y. F. Boosting the activity in the liquid-phase hydrogenation of S-containing nitroarenes by dual-site Pt/CeO_2 catalysts design. *Nat. Commun.* **2025**, *16*, 4851.
[26] Zhang, Q.; Zhang, M. Y.; Pan, Z. Y.; Li, D. C.; Tian, Z. B.; Ma, Y. F.; Gao, R.; Liu, J.; Wang, G. H. Seed-mediated engineering of dual-atom Ag-Pd synergy on CeO_2 for selective transfer hydrogenation of nitroarenes. *Appl. Catal. B: Environ. Energy* **2026**, *382*, 126019.
[27] Bai, S. X.; Yan, P. X.; Li, B. B.; Zhu, X. F.; He, L.; Kuang, M.; Yang, J. P. Mechanisms and challenges of nanoporous confinement for carbon dioxide electrocatalysis. *Nano Res.* **2026**, *19*, 94907935.
[28] Zhao, X. Y.; Khan, I. A.; Asif, M. B.; Zhang, Z. H. Nanoconfinement-based catalysis for advanced water treatment. *Appl. Catal. B: Environ. Energy* **2026**, *381*, 125877.
[29] Ma, Y. J.; Ou, P. F.; Wang, Z. Y.; Zhu, A. Q.; Lu, L. L.; Zhang, Y. H.; Zeng, W. X.; Song, J.; Pan, J. Interface engineering in CeO_2 (111) facets decorated with CdSe quantum dots for photocatalytic hydrogen evolution. *J. Colloid Interface Sci.* **2020**, *579*, 707–713.
[30] Wang, H. X.; Liao, B.; Lu, T.; Ai, Y. L.; Liu, G. Enhanced visible-light photocatalytic degradation of tetracycline by a novel hollow $BiOCl@CeO_2$ heterostructured microspheres: Structural characterization and reaction mechanism. *J. Hazard. Mater.* **2020**, *385*, 121552.
[31] Jiang, D.; Wang, W. Z.; Zheng, Y. L.; Zhang, L. Enhanced photon-to-electron conversion and improved water resistance of hydrogenated ceria in photocatalytic oxidation at gas-solid interface. *Appl. Catal. B: Environ.* **2016**, *191*, 86–93.
[32] Xia, H. H.; Dang, C. X.; Zhou, D.; Cai, W. Q. Lamellar cross-linking Ni/CeO_2 as an efficient and durable catalyst for dry reforming of methane. *Chem. Eng. J.* **2024**, *489*, 151365.
[33] Zhu, C. Z.; He, Q. Y.; Wang, W. K.; Du, F.; Yang, F.; Chen, C. X.; Wang, C. H.; Wang, S. B.; Duan, X. G. S-scheme photocatalysis induced by $ZnIn_2S_4$ nanoribbons-anchored hierarchical CeO_2 hollow spheres for boosted hydrogen evolution. *J. Colloid Interface Sci.* **2022**, *620*, 253–262.
[34] Yang, S. W.; Shen, H. D.; Cheng, F.; Wu, C.; Cao, Y. L.; Zhuo, S. F.; Zhang, Q. Y.; Zhang, H. P. Organometallic precursor induced defect-enriched mesoporous CeO_2 with high specific surface area: Preparation and catalytic performance. *J. Mater. Chem. A* **2020**, *8*, 14006–14014.
[35] Meng, Q. N.; Liang, X. L.; Guo, H.; Diao, Q.; Yu, X. J.; Xie, Z. W.; Wang, K.; Tang, Y. F.; Zhao, K. Facile preparation of CeO_2 and Co_3O_4 hollow composite with abundant oxygen vacancies and high surface area for improved acetone sensing. *Mater. Res. Bull.* **2024**, *170*, 112551.
[36] Nielsen, J. U.; Esplandiu, M. J.; Kolb, D. M. 4-Nitrothiophenol SAM on Au (111) investigated by *in situ* STM, electrochemistry, and XPS. *Langmuir* **2001**, *17*, 3454–3459.
[37] Haber, F. Über galvanisch gefälltes eisen. *Z. Elektrochem.* **1898**, *4*, 410–413.
[38] Zhao, Y. J.; Xu, T. H.; Bai, X. W.; Jia, Y.; Pan, Y. L.; Shi, X. W.; Zheng, H. J.; Zheng, L. X. Selective electrochemical hydrogenation of nitrobenzene to aniline coupled with efficient 5-hydroxymethylfurfural oxidation in aqueous electrolyte using a broccoli-like CuNi catalyst. *Chem. Eng. J.* **2024**, *482*, 149054.
[39] Zhang, P. J.; Gao, D. X.; Tang, X. Y.; Yang, X.; Zheng, H. Y.; Wang, Y. D.; Wang, X.; Xu, J. Q.; Wang, Z. J.; Liu, J. et al. Ordered van der waals hetero-nanoribbon from pressure-induced topochemical polymerization of azobenzene. *J. Am. Chem. Soc.* **2023**, *145*, 6845–6852.
[40] Pei, L. J.; Tan, H.; Liu, M. X.; Wang, R. Y.; Gu, X. M.; Ke, X. B.; Jia, J. F.; Zheng, Z. F. Hydroxyl-group-modified polymeric carbon nitride with the highly selective hydrogenation of nitrobenzene to N-phenylhydroxylamine under visible light. *Green Chem.* **2021**, *23*, 3612–3622.
[41] Wang, B. Q.; Deng, Z. R.; Li, Z. H. Efficient chemoselective hydrogenation of nitrobenzene to aniline, azoxybenzene and azobenzene over $CQDs/ZnIn_2S_4$ nanocomposites under visible light. *J. Catal.* **2020**, *389*, 241–246.
[42] Zhou, X. K.; Yang, Y.; Wang, J. B.; Ren, W. J.; Liu, S. J.; Zheng, C. H.; Gao, X. Enhancing nitrobenzene reduction to azoxybenzene by regulating the O-vacancy defects over rationally tailored CeO_2 nanocrystals. *Appl. Surf. Sci.* **2022**, *572*, 151343.
[43] Paterson, R.; Alharbi, H. Y.; Wills, C.; Chamberlain, T. W.; Bourne, R. A.; Griffiths, A.; Collins, S. M.; Wu, K. J.; Simmons, M. D.; Menzel, R. et al. Highly efficient and selective partial reduction of nitroarenes to N-arylhydroxylamines catalysed by phosphine oxide-decorated polymer immobilized ionic liquid stabilized ruthenium nanoparticles. *J. Catal.* **2023**, *417*, 74–88.
[44] Yuan, Z. L.; Gao, Y. J.; Tang, Q. J.; Wang, J. G.; Li, X.; Zhang, Z. H. Oxygen vacancies in β-MoO_3 mediate imine synthesis via reductive coupling of nitro compounds and alcohols. *Research* **2025**, *8*, 0993.
[45] Yuan, Z. L.; Huang, L.; Liu, Y. S.; Sun, Y.; Wang, G. H.; Li, X.; Lercher, J. A.; Zhang, Z. H. Synergy of oxygen vacancies and base sites for transfer hydrogenation of nitroarenes on ceria nanorods. *Angew. Chem., Int. Ed.* **2024**, *63*, e202317339.

This is an open access article under the terms of the Creative Commons Attribution 4.0 International License (CC BY 4.0, https://creativecommons.org/licenses/by/4.0/).

© The Author(s) 2026. Published by Tsinghua University Press.